Noninvasive and Simultaneous Imaging of Layer-Specific Retinal Functional Adaptation by Manganese-Enhanced MRI

Bruce A. Berkowitz,[1,2] *Robin Roberts,*[1] *Dennis J. Goebel,*[1] *and Hongmei Luan*[1]

Purpose. To test the hypothesis that high-resolution (23.4 μm intraretinal resolution) manganese-enhanced magnetic resonance imaging (MEMRI) can be used to noninvasively and simultaneously record from distinct layers of the rat retina cellular demand for ions associated with functional adaptation.

Methods. In control rats, high-resolution images were collected with or without systemic injection of $MnCl_2$ during light or dark adaptation; inner and outer retinal signal intensities were compared. In separate experiments, 1 month after systemic administration of $MnCl_2$ to awake dark-adapted control rats, possible toxic effects of Mn^{2+} on ocular health were assessed with the use of the following metrics: retinal layer thickness, intraocular pressure, and blood retinal barrier integrity.

Result. In nonmanganese-injected rats, the signal intensity difference between light and dark states for inner and outer retina was not significantly different ($P > 0.05$). In contrast, after manganese administration, the change in outer retinal signal intensity under light/dark conditions was significantly greater than that of inner retina. At 1 month after $MnCl_2$ injection, comparisons with controls revealed no evidence for deleterious ocular health effects as assessed by whole and inner retinal thickness, intraocular pressure, and blood retinal barrier integrity.

Conclusions. The present MEMRI examination was a safe (i.e., nontoxic) and relatively straightforward procedure that appeared to robustly reflect layer-specific retinal ion demand that correlates with normal retinal physiology responses associated with light and dark visual processing. Comprehensive MEMRI measures of retinal ion demand may be envisioned in a range of animal models for the study of normal development and aging. (*Invest Ophthalmol Vis Sci.* 2006;47:2668–2674) DOI: 10.1167/iovs.05-1588

Most of our understanding of retinal function has been obtained from studies of animals, including rodents, with the use of biochemical assessment, physiological recordings, and histochemical methodologies.[1,2] Although they generate useful basic knowledge, these experiments are invasive, do not provide adequate two-dimensional and three-dimensional spatial resolution, and can be nontrivial to perform. The rodent eye is particularly challenging for measuring retinal activity because of its compact laminar organization (10 distinct cellular and synaptic layers and two different circulations [retinal and choroidal]) contained within a thickness of 250 μm or less. This dense organization makes it hard to collect blood oxygen level–dependent (BOLD) functional magnetic resonance imaging (fMRI) or positron emission tomography data with high spatial resolution.

Metabolism in mammalian retinal cells is strongly linked with changes in the demand and subsequent distribution of ions. This metabolic–ion axis plays a central role in normal retinal function, including photoreceptor transduction, retinal neuronal transmitter release, regulation of gap-junction conductance, and modulation of postsynaptic potentials in retinal ganglion cells. However, current methods are unable to analytically and specifically measure in vivo normal changes in receptoral and postreceptoral ion demand with light/dark adaptation.

Recent studies in the brain have made use of manganese (Mn^{2+}) ion as an essential trace element, an ion surrogate, and a strong MRI contrast agent for functional manganese-enhanced MRI (MEMRI).[3] In these animal experiments, $MnCl_2$ was administered during a functional task performed outside the magnet, and the resultant accumulation and retention of Mn^{2+} ions in activated brain structures was subsequently detected noninvasively from the resultant enhancements evident in T_1-weighted MRI.[3,4] The spatial accuracy of MEMRI has been validated against the most common fMRI method, blood oxygenation level–dependent (BOLD) contrast, during a brain functional task.[5] MEMRI studies of function-dependent accumulation of Mn^{2+} ion has the further advantage of allowing acquisition of very high spatial resolution images with enhancements that are independent of changes in hemodynamics. It is not yet known whether similar MEMRI procedures could be applied to study normal retinal ion demand associated with a functional task such as light/dark adaptation.

In this study, we tested the hypothesis that high-resolution (23.4 μm intraretinal resolution) MEMRI can be used to accurately and precisely measure cellular demand for ions during light/dark adaptation simultaneously in the inner retina (containing ganglion cells and inner plexiform and inner nuclear layers) and the outer retina (containing outer nuclear layer and photoreceptors).

Methods

Animals were treated in accordance with the National Institutes of Health Guide for the Care and Use of Laboratory Animals and the ARVO Statement for the Use of Animals in Ophthalmic and Vision Research.

Light/Dark Adaptation

Sprague-Dawley rats (each weighing 200–250 g) were housed and maintained in normal laboratory lighting or total darkness for 20 hours. During dark adaptation, all procedures (e.g., weighing animal, injecting $MnCl_2$, anesthesia for MRI, and MRI examination) were conducted in

From the Departments of [1]Anatomy and Cell Biology and [2]Ophthalmology, Wayne State University, Detroit, Michigan.

Supported by National of Institutes of Health Grants EY013831 (BAB), Juvenile Diabetes Research Foundation (BAB), and EY014430 (DJG).

Submitted for publication December 14, 2005; revised January 20, 2006; accepted April 13, 2006.

Disclosure: **B.A. Berkowitz**, None; **R. Roberts**, None; **D.J. Goebel**, None; **H. Luan**, None

The publication costs of this article were defrayed in part by page charge payment. This article must therefore be marked "*advertisement*" in accordance with 18 U.S.C. §1734 solely to indicate this fact.

Corresponding author: Bruce A. Berkowitz, Department of Anatomy and Cell Biology, Wayne State University School of Medicine, 540 E. Canfield, Detroit, MI 48201; baberko@med.wayne.edu.

dim red light or darkness. $MnCl_2$ was administered as an intraperitoneal injection (44 mg/kg) to awake rats. These rats were maintained awake in light or dark conditions for another 3.5 hours, then anesthetized and imaged (MEMRI study), or they were returned to normal 12-hour cycled lighting conditions for another month (toxicity study).

Intraocular Pressure

Intraocular pressure (IOP) was measured with the use of a hand-held tonometer (Tonopen XL; Medtronic Ophthalmics, Jacksonville, FL). Ten to 15 readings were averaged per urethane-anesthetized rat.

MRI Data Acquisition

High-Resolution MRI. Immediately before the MRI experiment, rats were anesthetized using urethane (36% solution, intraperitoneally, 0.083 mL/20 g animal weight, prepared fresh daily; Aldrich, Milwaukee, WI). To maintain the core temperature, a recirculating heated water blanket was used. Rectal temperatures were continuously monitored throughout each experiment, as previously described.[6] Intraocular pressure was measured from each rat using a tonometer (Tonopen XL; Medtronic Ophthalmics). MRI data were acquired (4.7 T Avance; Bruker, Billerica, MA) system using a two-turn transmit/receive surface coil (1-cm diameter) placed over an eye. In some rats, left and right eyes were studied sequentially. Retinal thickness and signal intensity data were not different between left and right eyes (data not shown) and were respectively averaged for further analysis. Images were acquired using an adiabatic spin-echo imaging sequence (repetition time [TR], 350 seconds; echo time [TE], 16.7 milliseconds; number of acquisitions [NA], 16; sweep width, 61,728 Hz; matrix size, 256 × 512; slice thickness, 600 μm; field of view, 12 × 12 mm^2; 23 minutes/image).[7] A single transverse slice through the center of the eye (based on sagittal localizer images collected using the same adiabatic pulse sequence described) was obtained for each rat.

Toxicity Studies. Dark-adapted control rats were injected intraperitoneally with manganese chloride 1 month before the study. Four hours after injection, rats were returned to ambient laboratory/lighting and were then studied 1 month later to determine the potential for Mn^{2+}-induced toxicity in the retina using the following metrics.

Blood-Retinal Barrier Integrity. Rats were prepared for the MRI experiment, as described. Animals were allowed to breathe spontaneously during the experiment. DCE-MRI data were generated and analyzed to calculate the blood-retinal barrier (BRB) integrity, as previously described.[8] Briefly, after anesthetizing and preparing the rat, a 25-gauge tail vein catheter used to deliver contrast agent was positioned and secured. Sequential spin-echo imaging data were collected (TR, 1 second; TE, 22.7 milliseconds; NA, 1; matrix size, 128 × 256; slice thickness, 1 mm; field of view, 32 × 32 mm^2; sweep width, 25,000 Hz; 2 minutes per image). Representative images in the rat obtained using these acquisition parameters were previously published.[9] Twelve sequential 2-minute images were acquired—three control images before injection of contrast agent and nine images during and after a 6-second gadolinium diethylenetriamine pentaacetic acid (Gd-DTPA) bolus injection. The dose of contrast agent (Gd-DTPA; Magnevist; Berlex Laboratories, Wayne, NJ) was 0.1 mM Gd-DTPA/L per kilogram. In each animal, Gd-DTPA was injected at the same phase encode step collected near the beginning of the fourth image. All rats were humanely killed by injection of intracardiac potassium chloride, and their eyes were removed for histologic examination.

Histology. After initial overnight fixation in formalin at 4°C, eyecups were postfixed for 3 hours on ice in 0.67% osmium tetroxide and 0.83% glutaraldehyde in 0.1 M sodium phosphate buffer (pH 7.4). Eyecups were then rinsed with 0.1 M phosphate buffer, dehydrated in graded ethanols and propylene oxide, and embedded in Epon araldite. Semithick (1.5 mm) radial sections through the optic nerve head were cut with an ultramicrotome (Reichert-Jung Ultracut E; Cambridge Instruments, Buffalo, NY), contrasted with Richardson's stain, and coverslipped for histopathologic evaluation of retinal layer thickness.

Data Analysis

Retinal Thickness. Based on the MRI data, inner or total retinal thicknesses were measured, respectively, as the radial distance between the anterior edge and the middle edge (defined by its change in signal intensity) or the posterior edge of the retina at distances ± 0.4 – 1 mm from the optic nerve. Mean superior and inferior values generated for each rat were used for comparisons. The difference in the number of sample *n*'s reflects the fact that data were not collected from all rats because some had ill-defined retinal boundaries.

Inner or total retinal thicknesses were also assessed from histologic data. In this case, thicknesses were measured from camera lucida tracings of representative and spatially calibrated median slices at distances ± 0.4 – 1 mm from the edges of the optic nerve.

MEMRI. Intraretinal signal intensity was analyzed using IMAGE (a public domain image processing and analysis program available at http://rsb.info.nih.gov/nih-image/ [accessed March 17, 2006]) and derived macros.[10] In these initial studies, we controlled for changes in receiver gain differences between animals by normalizing the signal intensity of a fixed region of noise in each rat to a fixed value. Other tissues within the sensitive volume of the coil demonstrated enhancement after manganese injection and thus were considered inadequate as internal references. Inner and outer signal intensity data (from the edge of the optic nerve to 1 mm from the center of the optic nerve) were extracted.

Blood-Retinal Barrier Integrity. These data were analyzed as previously described.[8] Briefly, movement within the slice plane was corrected using a warp affine image coregistration for each animal using software written in-house. After coregistration, the MRI data were transferred to a computer (Power Mac G4; Apple, Cupertino, CA) and were analyzed using the program IMAGE. For each pixel, the fractional signal enhancement, E, was calculated: $E = (S(t) - S_0)/S_0$, where $S(t)$ is the pixel signal intensity at time t after contrast and S_0 is the precontrast signal intensity (measured from the average of the three control images) at the same pixel spatial location. Because no increase in vitreous signal intensity was found after Gd-DTPA injection, we did not calculate a BRB permeability surface area product in this study. For the calculation of signal enhancement, a region of interest (ROI) was chosen that contained the entire vitreous space. The area of this ROI and the mean E within the ROI were measured at each postcontrast time point. In one rat, subtle movement generated ghosting artifacts in the phase encode direction of one of the images. Such artifacts are discernible as random noise by visual inspection and can reduce precision. This particular time point was not included in the final data analysis.

Statistical Analysis

Retinal thickness and IOP data were consistent with a normal distribution, and comparisons between groups were performed using unpaired, 2-tailed t test analysis. For BRB measurements, analysis of covariance (ANCOVA) was performed on temporal evolution data for control and manganese-exposed rats. Comparisons of MEMRI retinal signal intensities were performed using ANCOVA on the spatial maps of average signal intensity change as a function of distance from the optic nerve (from the edge of the optic nerve to 1 mm from the center of the optic nerve) and a generalized estimating equation (GEE) approach.[11] GEE performs general linear regression analysis using all the pixels in each subject and accounts for the within-subject correlation between adjacent pixels. In all cases, $P < 0.05$ was considered statistically significant.

Results

Systemic Physiology during MRI Examination

Summaries of body weights and core temperatures during the MRI experiments are presented in Table 1. Core temperatures during MRI examinations were maintained in all groups; no

Table 1. Summary of Animal Body Weights and Core Temperatures

Group	Weight (g)	Core Temperature (°C)
Light adapted ($n = 7$)	219.0 ± 5.2	36.6 ± 0.1
Dark adapted ($n = 7$)	217.0 ± 3.8	36.4 ± 0.2
Light adapted, MEMRI ($n = 5$)	232.6 ± 1.7	36.7 ± 0.2
Dark adapted, MEMRI ($n = 5$)	224.8 ± 6.3	36.5 ± 0.3

Values are mean ± SEM.

significant differences ($P > 0.05$) were observed between any of the groups.

High-Resolution MRI without $MnCl_2$ Injection

As illustrated in Figure 1, high-resolution T_1-weighted images of normal rat eye (i.e., not exposed to $MnCl_2$) revealed a distinct retinal laminar pattern. In these control animals, light and dark adaptation did not elicit a change in MRI-derived total retinal thickness ($P > 0.05$; 211.4 ± 2.2 μm [$n = 8$] and 209.8 ± 2.0 μm [$n = 7$], respectively; mean ± SEM) or inner retinal thickness ($P > 0.05$; 109.7 ± 6.6 μm [$n = 4$] and 111.0 ± 4.6 μm [$n = 3$], respectively). These inner retinal thickness values agreed with those in the literature for the combined thickness of retinal ganglion cell, inner plexiform, and inner nuclear layers in control rats (107 ± 3 μm).[12] The outer retina (combined thickness of the outer nuclear and photoreceptor layers) was less well defined with these acquisition parameters but could be identified by comparing MEMRI data of light- and dark-adapted rats.

As seen in Figures 2 and 3, in the absence of Mn^{2+}, light and dark conditions produced different ($P < 0.05$) signal intensities for inner retina (61.5 ± 0.9 a.u. [$n = 7$] and 69.5 ± 0.7 a.u. [$n = 7$], respectively) and outer retina (52.1 ± 1.0 a.u. [$n = 7$] and 57.8 ± 0.7 a.u. [n = 7], respectively). However, the intensity difference between light and dark states for inner and outer retina (i.e., 11% and 10%, respectively) was not significantly different ($P > 0.05$).

MEMRI

Four hours after intraperitoneal $MnCl_2$, signal enhancements consistent with retention of Mn^{2+} ion were evident throughout the retina (Fig. 2). In these experiments, no change ($P > 0.05$) between control and $MnCl_2$-injected rats in whole retinal thickness between light and dark adaptation was found ($P > 0.05$; 208.0 ± 6.1 μm [$n = 4$] and 210.3 ± 4.7 μm [$n = 4$], respectively).

As seen in Figure 4, in the presence of Mn^{2+}, light and dark conditions produced different ($P < 0.05$) signal intensities for inner retina (104.3 ± 1.2 a.u. [$n = 5$] and 110.2 ± 0.8 a.u. [$n = 5$], respectively) and outer retina (86.0 ± 1.4 a.u. [$n = 5$] and 107.3 ± 1.0 a.u. [$n = 5$], respectively). The intensity difference between light and dark adaptation for inner and outer retina (6% and 25%, respectively) were significantly different ($P < 0.0001$; Fig. 4).

Toxicity Studies

Potential toxic effects of Mn^{2+} exposure were also evaluated. We did not observe any rat deaths after Mn^{2+} injection in any of the groups. At 1 month after Mn^{2+} injection, no significant ($P > 0.05$) differences were found between histology and MRI-derived whole retinal thickness (183.9 ± 11.8 [$n = 5$] vs. 189.8 ± 6.9 [$n = 5$] μm, respectively) or inner retinal thickness (90.8 ± 7.1 [$n = 4$] vs. 103.0 ± 6.2 [$n = 4$] μm, respectively). In addition, no significant ($P > 0.05$) differences between Mn^{2+}-treated and control rats were found in various parameters of ocular health, such as MRI-derived whole and inner retinal thickness measurements and IOP (Fig. 5). After contrast agent administration, a significant ($P < 0.05$) difference in temporal evolution of vitreous signal intensity changes between control and manganese-exposed rats was found. This difference was not considered to indicate toxicity given that

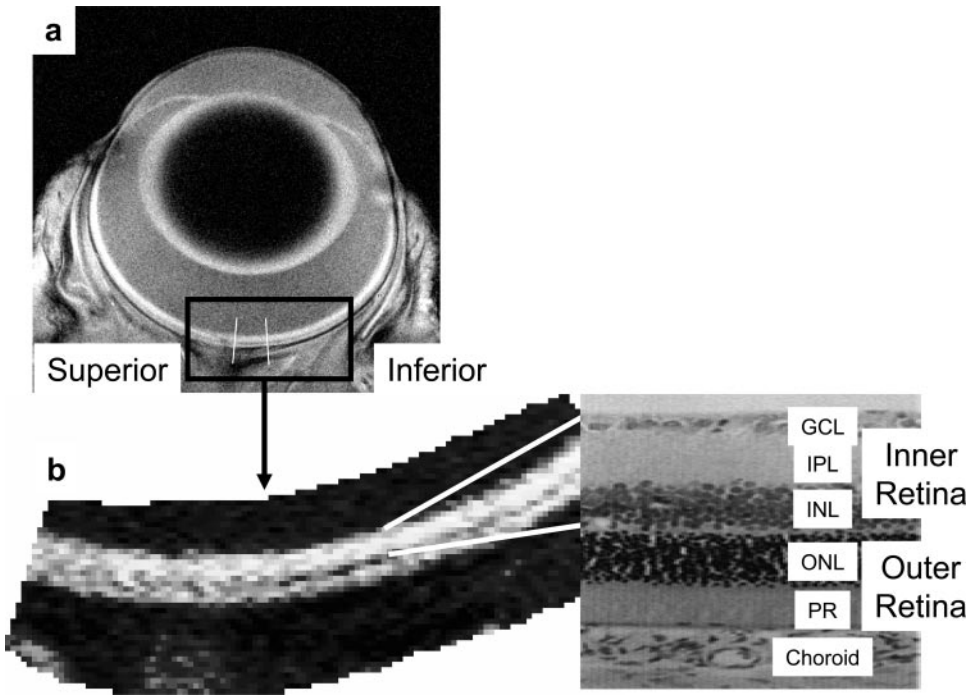

Figure 1. High-resolution MRI of retinal anatomy without $MnCl_2$ injection. (**a**) Representative image (46.8 × 23.4 × 600 μm^3) from a spontaneously breathing anesthetized rat without administration of $MnCl_2$. The *white* band in the posterior region of the eye represents the retina. The inferior retinal region, from which retinal thicknesses were measured, is also indicated (*lines*) nearly perpendicular to the retina. A similar region was measured superiorly but is not shown. (**b**) Magnified region-of-interest image showing the distinctness of the retinal layers (i.e., inner and outer retina). Note that the contrast settings were changed between (**a**) and (**b**) to better highlight the intraretinal layers. Total retinal thickness was not a function of light or dark adaptation and was in agreement with values derived from the literature in a variety laboratories using ex vivo methods in different rat strains and at different ages.[12,23] *Inset, bottom right*: the innermost retinal layer corresponds in thickness to the combined width of the retinal ganglion cell (GC), inner plexiform (IP), and inner nuclear (IN) layers on histologic analysis. The layers of the outer retina (i.e., outer nuclear [ON], photoreceptor [PR], and choroidal circulation [choroid]) are also defined.

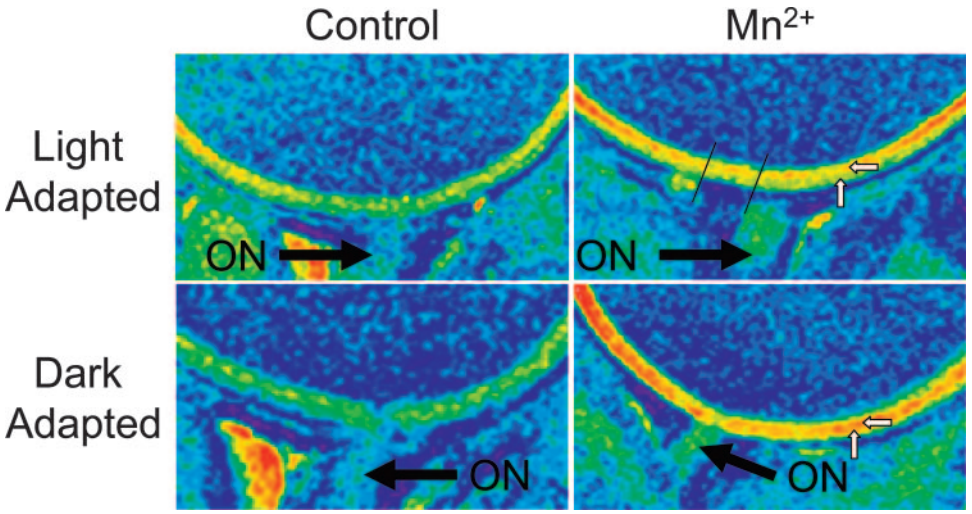

FIGURE 2. Visualization of MEMRI retinal adaptation. Pseudocolor-magnified region of interest of smoothed representative images ($46.8 \times 23.4 \times 600\ \mu m^3$) from four spontaneously breathing anesthetized rats not injected with $MnCl_2$ (*left*) or 4 hours after systemic injection of $MnCl_2$ (*right*). The optic nerve (ON) is identified in each image (*black arrows*). All images were scaled similarly and used the same color scheme. The superior retinal region from which signal intensities were measured is indicated by *black lines* nearly perpendicular to the retina. A similar region was measured inferiorly but is not shown. Retinal colors (*green* to *yellow* to *red*) represented lowest to highest signal intensities. After $MnCl_2$ injection, the inner retina (*horizontal white arrow*) was clearly enhanced during light and dark adaptation, whereas enhancement of the outer retina (*vertical white arrow*) was visually more evident during dark adaptation than during light adaptation.

both groups had values that agreed with those previously reported for intact BRB, and, more important, the values of the manganese groups were consistently lower than those of the control[8] (Fig. 5).

DISCUSSION

In this study, we report for the first time evidence that inner and outer retinal MEMRI patterns reflect known changes in retinal layer–specific ion demand during functional adaptation in the rat. In this initial report, we thought it reasonable to refer to Mn^{2+} as a general cation surrogate without focusing specifically on which ions it may or may not be tracking given that the particular ion species could change depending on the situation or even the retinal layer. We speculate that Mn^{2+} likely tracks Ca^{2+} ion movement, but we did not perform experiments to support this notion. It is well established that rod and cone photoreceptors depolarize (i.e., release glutamate) in the dark and hyperpolarize in response to light. The latter is caused by the closure of the cGMP-gated ion channels by way of the phototransduction cascade, which leads to a reduction in their graded potential, a decrease in glutamate release, and a buildup of ions such as sodium and calcium. Thus, the activity and ion demand of photoreceptors are increased in the dark and attenuated in the light. In this study, a significantly greater uptake of manganese in outer retina was found in dark adaptation relative to that in the light. In the inner retina, the situation is more complex. The output of the outer retina is divided equally into a light-driven pathway, known as the ON pathway, and a dark-driven pathway, known as the OFF pathway.[13] It is at the bipolar level that the ON and OFF pathways are formed through sign-conserving action of ionotropic glutamate receptors, which signal the OFF pathway (through OFF bipolar cells), and the sign-inverting response

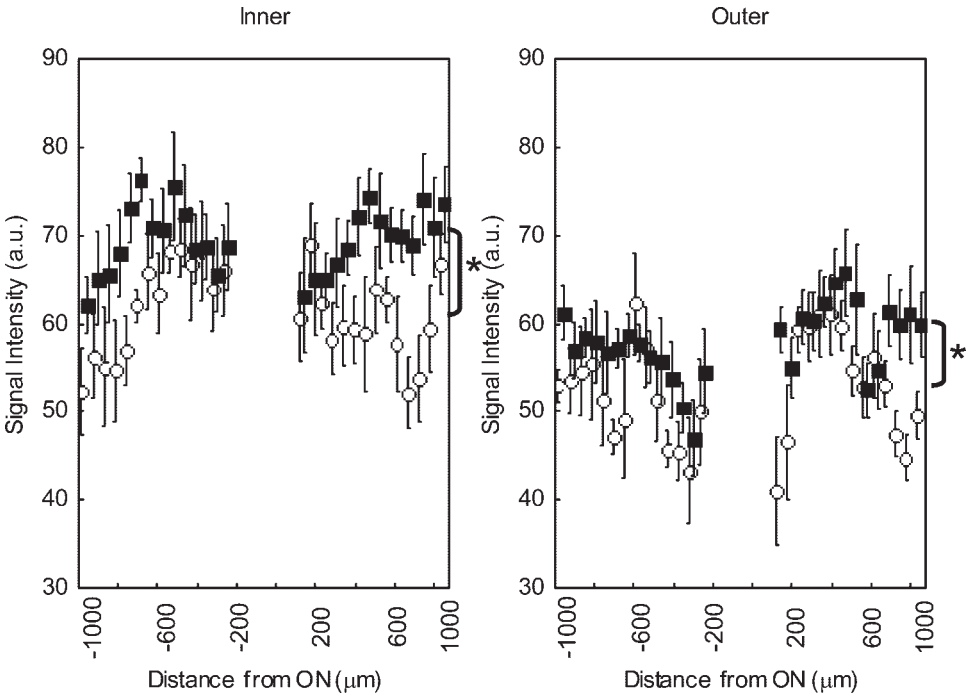

FIGURE 3. Baseline changes in inner (*left*) and outer (*right*) signal intensity with light (○, $n = 7$) and dark (■, $n = 7$) adaptation from the edge of the optic nerve to 1 mm from the center of the optic nerve. Each data point represents the average of intensities from that spatial location. Error bars, SEM (indicated by the *asterisk*), and ANCOVA showed differences between *y*-intercepts at the $P < 0.05$ level. GEE analysis confirmed these findings.

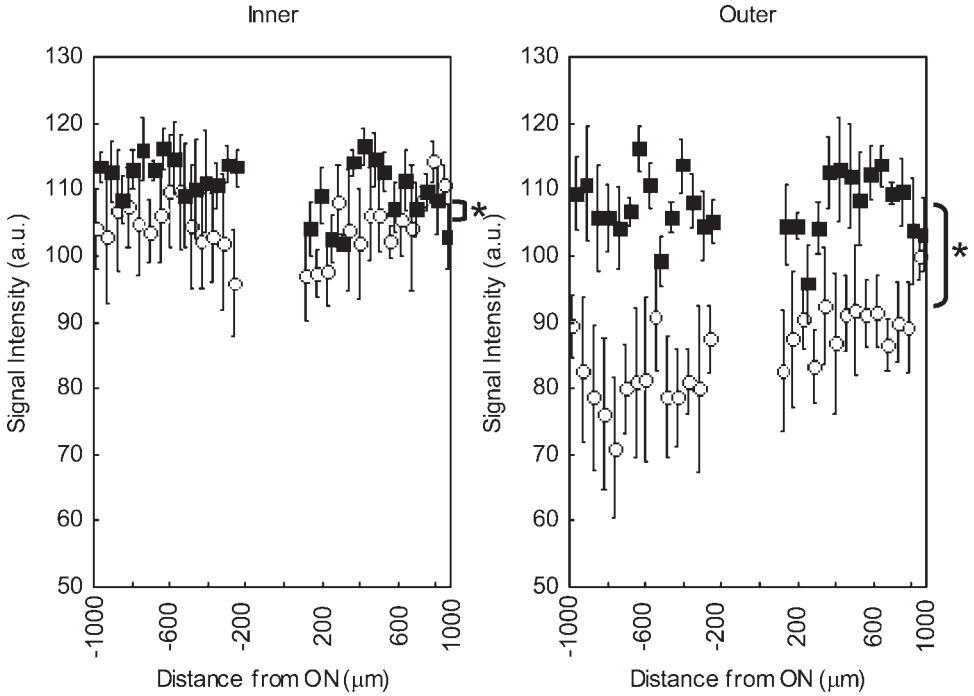

FIGURE 4. MEMRI changes in inner (*left*) and outer (*right*) signal intensity with light (○, $n = 5$) and dark (■, $n = 5$) adaptation from the edge of the optic nerve to 1 mm from the center of the optic nerve 4 hours after intraperitoneal systemic administration of $MnCl_2$. Each data point represents the average of intensities from that spatial location. Error bars, SEM (indicated by the *asterisk*), and ANCOVA showed differences between *y*-intercepts at the $P < 0.05$ level. GEE analysis confirmed these findings.

through metabotropic glutamate receptors, which signal the ON pathway (through ON bipolar cells).[14] Thus, when the retina is dark adapted, the OFF pathway (OFF bipolar cell to OFF ganglion cell) is active in the inner retina; conversely, in the light, the ON pathway (ON bipolar cell to ON ganglion cell) is depolarizing. With equal representation of ON and OFF cells (bipolar and ganglion cells) in the retina, changes in inner retina activity caused by light or dark adaptation would be expected to be relatively equal. Indeed, in the present study, we found changes in signal intensity in inner retina between light and dark adaptation that were on the order of the baseline changes and were significantly ($P < 0.05$) smaller than those found in outer retina. We do not yet understand the significance of the apparent offset in superior signal intensities in outer retina (Fig. 4). This offset does not appear to be related to the use of the surface coil since it is found (Figs. 2, 3) in only one condition (dark outer retina) and not in the others.

The light/dark intraretinal MEMRI pattern does not appear to result from manganese-induced toxicity. Although the precise mechanisms by which Mn^{2+} is transported and retained in the retina are unknown, toxicity associated with Mn^{2+} ion exposure appears to be a dose-dependent phenomenon. This is

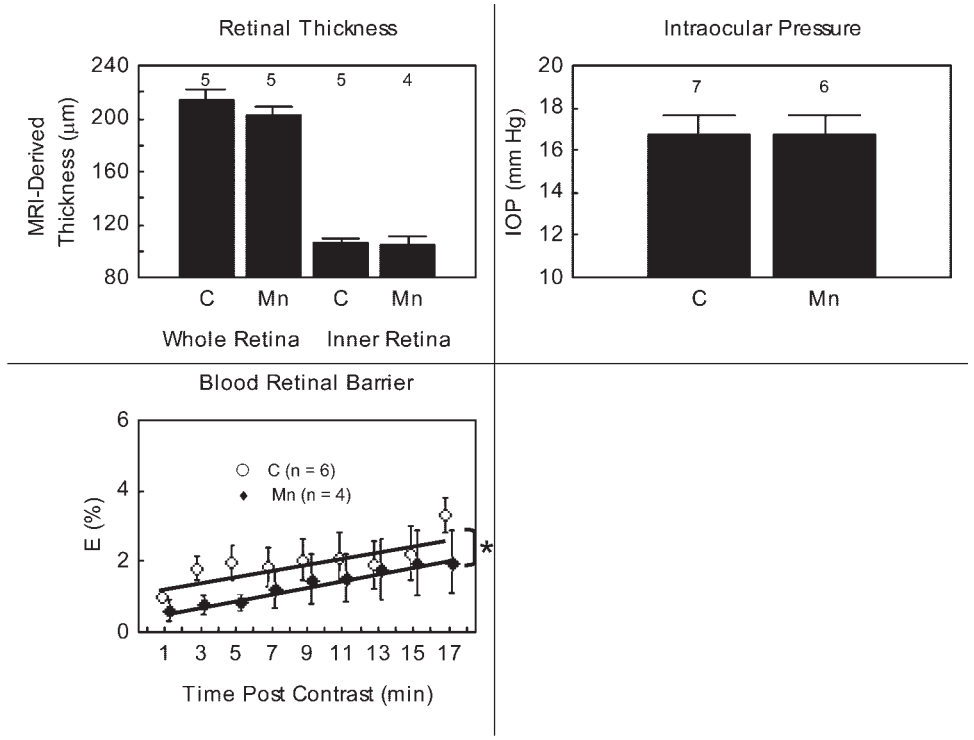

FIGURE 5. Summary of the following parameters 1 month after systemic $MnCl_2$ injection as compared with control rats. *Upper left*: MRI-derived whole and inner retinal thickness. *Upper right*: IOP as measured by a handheld tonometer (Tonopen XL) unit before the MRI experiment. *Lower left*: BRB integrity. Note that no significant ($P > 0.05$) change from respective control values was found for thickness or IOP. A significant difference ($^*P < 0.05$) in change in vitreal signal intensity after the injection of contrast agent was found between control and manganese-exposed animals, though the values of the manganese group were consistently lower than those of the control group. Error bars represent SEM, and numbers above the bars represent number of animals studied.

a feature shared with another activity-related tracer, 2-deoxyglucose. In this case, low concentrations of accumulated 2-deoxyglucose can be used as a nontoxic reporter of local activity, whereas high injected levels can be toxic. Higher doses of $MnCl_2$ (i.e., 70 mg/kg) than those used in this study (44 mg/kg) are not reported to be toxic or associated with abnormal behavior after 3 months.[4] In this study, we found no evidence for toxicity as measured by various metrics of ocular health (retinal thickness, intraocular pressure, BRB integrity) at 1 month after $MnCl_2$, even though our preliminary data in a few animals suggest that Mn^{2+} is retained in retinal neurons because substantial intraretinal enhancements were still evident 1 month after injection (data not shown). Previous work has confirmed that Mn^{2+} is retained in neuronal tissue for relatively long periods.[15] These data support our contention that at the present dose, $MnCl_2$ is safe (i.e., not toxic).

Some methodological limitations of this initial account were considered. First, manganese uptake was evaluated at a single time point, so information about the temporal evolution of manganese transport was unavailable. We could have countered this in either of two ways: collect sequential MRI data while the rat is in the magnet the entire time, or use higher injected doses of manganese. However, each approach would have increased the likelihood of confounding data interpretation by an anesthetic effect, motion artifact, or retinal toxicity and, hence, were not used in this study. We also chose not to quantify tissue manganese levels from the MRI data because of the uncertainties about the physical chemistry parameters associated with the ligation of intracellular manganese.[16] We also made the assumption that in vivo retinal signal intensities were linearly related to manganese concentration.[17,18] This linear response assumption appears reasonable because no evidence was found for signal intensity losses that would be expected from manganese-induced T_2 shortening in the retina. It is expected that future investigators—perhaps using higher field strengths, stronger gradient sets, or different stimulation procedures—will be able to resolve Mn^{2+} ion uptake in distinct cellular layers within the retina.

Surprisingly, in the absence of manganese, baseline signal intensity changes were observed in the inner and outer retina between light and dark states (Fig. 3). The reason for this apparent light-induced baseline change is unclear. It is possible that changes in, for example, intraretinal pH, retinal perfusion, or both between light and dark conditions might have subtly changed the chemical composition within the retina, thereby altering the relaxation properties of each layer.[19,20] Alternatively, baseline differences could have represented a systematic error reflecting a bias in how the rats were handled between light and dark conditions. Regardless, for the purposes of this study, the key question was whether these non-Mn^{2+} light/dark baseline changes contained intraretinal functional adaptation/ion demand information. As discussed, relatively large changes occurred in outer retina physiology and ion demand between light and dark adaptation compared with those of the inner retina. However, the baseline changes reported here do not reflect this known physiology because both inner and outer retina changed by similar ($P > 0.05$) degrees. This observation raises the possibility of a non–ion demand-dependent mechanism underlying the baseline changes. More work is needed to understand the subtle change in baseline signal intensity between light and dark adaptation.

To date, MRI evaluation of retinal function has been limited to a single study by Duong et al.[21] using BOLD-based fMRI. In that study, retinal function was dynamically imaged in cats. However, proper implementation of the BOLD experiment in cats was found to be challenging, and similar studies in the eyes of rats and mice, which are smaller, will likely present additional challenges. Furthermore, separate BOLD signals from retinal and choroidal circulations have not been distinguished, making interpretation of the functional changes difficult. In contrast, the MEMRI approach described in this study provides high-resolution images in vivo while simultaneously recording a layer-specific history of ion demand activity that occurred in the retina of awake animals, independent of changes in hemodynamics.

Early MEMRI studies of brain function were performed in anesthetized rats with cannula insertion and mannitol coinjection to transiently break the blood-brain barrier and allow Mn^{2+} ion to enter the brain.[3] In these early experiments, activity was only detected when blood-brain barrier integrity was lost. More recently, after 24 hours of stimulation in awake mice, Yu et al.[4] reported activity-related enhancement patterns in the brain after intraperitoneal injection of $MnCl_2$. However, the MEMRI enhancements were observed only in some brain areas and were a function of dose, time after injection, and distance from the blood supply or ventricles (i.e., brain regions closer to the blood supply were exposed to higher Mn^{2+} ion levels and were enhanced to a larger degree). In the present study, we found a more extensive uptake pattern of Mn^{2+} in the retina than was reported in the brain, possibly because the retina is highly vascularized and relatively thin and has smaller diffusion distances than are found in the brain.

We expect that MEMRI will prove useful for analyses of changes in retinal ion demand associated with functional adaptation in studies of postnatal development and aging, and we speculate that MEMRI will also be valuable for measuring changes in ion demand in a wide range of disease models (including diabetic retinopathy, retinopathy of prematurity, glaucoma, and retinitis pigmentosa) in healthy and surgically, biochemically, or genetically altered animals. In addition, high-resolution MEMRI adaptation maps of the retina can be readily combined with noninvasive MRI measures of retinal thickness and BRB integrity.[8,22]

Acknowledgments

The authors thank Rod Braun, Tim Kern, Donald A. Fox, Gary Trick, Zhuo-Hau Pan, and Alan Koretsky for helpful discussions and for review of this manuscript.

References

1. Wang L, Kondo M, Bill A. Glucose metabolism in cat outer retina: effects of light and hyperoxia. *Invest Ophthalmol Vis Sci*. 1997; 38:48–55.
2. Winkler BS, Pourcho RG, Starnes C, Slocum J, Slocum N. Metabolic mapping in mammalian retina: a biochemical and ^{3}H-2-deoxyglucose autoradiographic study. *Exp Eye Res*. 2003;77:327–337.
3. Lin YJ, Koretsky AP. Manganese ion enhances T1-weighted MRI during brain activation: an approach to direct imaging of brain function. *Magn Reson Med*. 1997;38:378–388.
4. Yu X, Wadghiri YZ, Sanes DH, Turnbull DH. In vivo auditory brain mapping in mice with Mn-enhanced MRI. *Nat Neurosci*. 2005;8: 961–968.
5. Duong TQ, Silva AC, Lee SP, Kim SG. Functional MRI of calcium-dependent synaptic activity: cross correlation with CBF and BOLD measurements. *Magn Reson Med*. 2000;43:383–392.
6. Berkowitz BA, Ito Y, Kern TS, McDonald C, Hawkins R. Correction of early subnormal superior hemiretinal DeltaPO(2) predicts therapeutic efficacy in experimental diabetic retinopathy. *Invest Ophthalmol Vis Sci*. 2001;42:2964–2969.
7. Schupp DG, Merkle H, Ellermann JM, Ke Y, Garwood M. Localized detection of glioma glycolysis using edited 1H MRS. *Magn Reson Med*. 1993;30:18–27.
8. Berkowitz BA, Roberts R, Luan H, Peysakhov J, Mao X, Thomas KA. Dynamic contrast-enhanced MRI measurements of passive perme-

ability through blood retinal barrier in diabetic rats. *Invest Ophthalmol Vis Sci*. 2004;45:2391–2398.

9. Berkowitz BA, Kowluru RA, Frank RN, Kern TS, Hohman TC, Prakash M. Subnormal retinal oxygenation response precedes diabetic-like retinopathy. *Invest Ophthalmol Vis Sci.* 1999;40:2100–2105.
10. Berkowitz BA. Adult and newborn rat inner retinal oxygenation during carbogen and 100% oxygen breathing: comparison using magnetic resonance imaging delta Po2 mapping. *Invest Ophthalmol Vis Sci*. 1996;37:2089–2098.
11. Liang Z. Longitudinal data analysis using generalized linear models. *Biometrika*. 1986;73:13–22.
12. Hughes WF. Quantitation of ischemic damage in the rat retina. *Exp Eye Res*. 1991;53:573–582.
13. Murakami M, Otsuka T, Shimazaki H. Effects of aspartate and glutamate on the bipolar cells in the carp retina. *Vision Res*. 1975;15:456–458.
14. Yamashita M, Wassle H. Responses of rod bipolar cells isolated from the rat retina to the glutamate agonist 2-amino-4-phosphonobutyric acid (APB). *J Neurosci*. 1991;11:2372–2382.
15. Valois AA, Webster WS. Retention and distribution of manganese in the mouse brain following acute exposure on postnatal day 0, 7, 14 or 42: an autoradiographic and gamma counting study. *Toxicology*. 1989;57:315–328.
16. London RE, Toney G, Gabel SA, Funk A. Magnetic resonance imaging studies of the brains of anesthetized rats treated with manganese chloride. *Brain Res Bull*. 1989;23:229–235.
17. Liu CH, D'Arceuil HE, de Crespigny AJ. Direct CSF injection of MnCl(2) for dynamic manganese-enhanced MRI. *Magn Reson Med*. 2004;51:978–987.
18. Li SK, Jeong EK, Hastings MS. Magnetic resonance imaging study of current and ion delivery into the eye during transscleral and transcorneal iontophoresis. *Invest Ophthalmol Vis Sci*. 2004;45:1224–1231.
19. Feke GT, Zuckerman R, Green GJ, Weiter JJ. Response of human retinal blood flow to light and dark. *Invest Ophthalmol Vis Sci*. 1983;24:136–141.
20. Padnick-Silver L, Linsenmeier RA. Quantification of in vivo anaerobic metabolism in the normal cat retina through intraretinal pH measurements. *Vis Neurosci*. 2002;19:793–806.
21. Duong TQ, Ngan SC, Ugurbil K, Kim SG. Functional magnetic resonance imaging of the retina. *Invest Ophthalmol Vis Sci*. 2002;43:1176–1181.
22. Trick GL, Berkowitz BA. Retinal oxygenation response and retinopathy. *Prog Retin Eye Res*. 2005;24:259–274.
23. Buttery RG, Hinrichsen CF, Weller WL, Haight JR. How thick should a retina be? A comparative study of mammalian species with and without intraretinal vasculature. *Vision Res*. 1991;31:169–187.